

## EFFECT OF SMEARED ${}^4\text{He}$ -CORE IN ${}^6\text{He} + p$ ELASTIC SCATTERING\*

DHRUBA GUPTA, C. SAMANTA AND RITUPARNA KANUNGO†

Saha Institute of Nuclear Physics  
1/AF, Bidhannagar, Calcutta 700064, India

(Received November 20, 1999)

The elastic scattering data of  $p+{}^4,{}^6\text{He}$ , available in the 40A–45A MeV energy range have been analyzed in a microscopic framework using an isospin, density and momentum-dependent finite-range effective interaction in a single folding model. The folded potentials explain the  $p+{}^4\text{He}$  angular distribution data. For  ${}^6\text{He}$ , several density prescriptions of varied rms radii are employed. All these prescriptions lead to almost same fit to the  ${}^6\text{He} + p$  elastic angular distribution data with slight variations of the imaginary strength. Microscopic calculations assuming proton scattering from the smeared  ${}^4\text{He}$ -core in  ${}^6\text{He}$ , ignoring the halo, can also reproduce the experimental data if the strength of the imaginary part of the microscopic potential is enhanced. Implications of these results are discussed.

PACS numbers: 25.40.Cm, 25.60.-t, 21.45.+v, 21.10.Gv

### 1. Introduction

Recent studies [1–4] on the neutron-halo nucleus  ${}^6\text{He}$  have suggested that it has a  ${}^4\text{He} + 2n$  structure, although ambiguity persists in determination of its root-mean-square (rms) radius. Its low  ${}^4\text{He} + 2n$  breakup threshold (0.975 MeV) [5] insinuates a long tail in its wave function. Tanihata *et al.* [4] claimed that the core  ${}^4\text{He}$  essentially remains unmodified inside  ${}^6\text{He}$  and the two neutrons form either a halo or a skin of  ${}^6\text{He}$ . From static density Glauber model calculations of reaction cross sections, it was shown that the rms matter radius of  ${}^6\text{He}$  is  $R_m \simeq 2.33$  fm. The rms neutron radius ( $R_n \simeq 2.59$  fm) of  ${}^6\text{He}$  was found to be larger than the proton radius ( $R_p \simeq 1.72$  fm), delineating an extended neutron density distribution, far beyond the proton one. Al-Khalili *et al.* [6] considered corrections to this static density Glauber

---

\* Presented at the XXVI Mazurian Lakes School of Physics, Krzyże, Poland September 1–11, 1999.

† Present address: RIKEN, 2-1 Hirosawa, Wako, Saitama 351-0198, Japan

model calculations and showed that if the granular structure of the projectile is represented by more realistic few-body wave functions, it increases  $R_m$  to 2.71 fm. Several other theoretical models predicted [6–9] different rms radius of  ${}^6\text{He}$  in the range of 2.32 fm to 2.76 fm adding further confusion to this topic. Recently  ${}^6\text{He} + p$  elastic scattering data have been available at 41.6A MeV [10], providing an opportunity to test the validity of these various prescriptions with the help of folded potentials, which explicitly incorporate the structure of the interacting nuclei.

We have reanalyzed the elastic scattering data of  ${}^6\text{He} + p$  at 41.6A MeV [10], in a microscopic folding model using more realistic density distributions and an effective nucleon–nucleon interaction which, in addition to being finite-range, momentum and density dependent, has an explicit isospin dependence. Available 40A and 45A MeV  $p+{}^4\text{He}$  scattering data [11,12] have also been analyzed on equal footing to understand the role of  ${}^4\text{He}$  as a core in  ${}^6\text{He}$ . Different density prescriptions of  ${}^6\text{He}$  are used with a hope to pinpoint its rms radius.

## 2. Analysis

For single folding model calculations we use the SBM (Modified Seyler Blanchard) interaction, which has different strengths for  $pp$ ,  $nn$  and  $pn$  interactions [13]. The  ${}^6\text{He}$  ground state densities used are obtained by using Faddeev wave function models called, P1, FC, FC6, Q3, Q1, FB, FA, K, C [6,7,14]. These models incorporate different  $n$ – $n$  and  $n$ – $\alpha$  potentials with a variation of two-neutron separation energy  $E(2n)$  from about  $-1.15$  MeV to  $-0.21$  MeV and thereby a variation of rms radii of  ${}^6\text{He}$ . The rms radii corresponding to the above models are 2.32, 2.50, 2.53, 2.54, 2.56, 2.64, 2.64, 2.66, 2.76 fm respectively. These radii are computed assuming that the bare  ${}^4\text{He}$  core rms radius is 1.49 fm [7]. However, the  ${}^4\text{He}$  inside  ${}^6\text{He}$  is smeared due to its motion with respect to the center of mass of  ${}^6\text{He}$ . The density of the smeared core is taken as the difference between the  ${}^6\text{He}$  and  $2n$ -halo densities, the rms radius being different for different prescriptions. Since the isospin sensitive interaction requires separate proton and neutron densities, we have constructed them from the available  ${}^6\text{He}$  models [6,7,14]. For the  $p$ – ${}^4\text{He}$  scattering, they were formulated from the bare core density distribution of  ${}^4\text{He}$  [7]. In the microscopic calculations both the real ( $V$ ) and imaginary ( $W$ ) parts of the folded potentials are assumed to have the same shape, *i.e.*  $V_{\text{micro}}(r) = V + iW = (N_R + iN_I)U$  where,  $U$  is the folded potential, and  $N_R$ ,  $N_I$  are the renormalization factors for real and imaginary parts respectively [15].

For comparing the results, a phenomenological optical model (OM) analysis of the data is first carried out, the best fit parameters (Table I) and the respective Woods–Saxon and folded potentials (Fig. 1(a)–(c)) are shown.

TABLE I

Optical potential parameters used in  $p$ -nucleus elastic scattering  $r_c = 1.40$  fm,  $R_x = r_x A_T^{1/3}$

Nucleus	E/A (MeV)	$V_o$ (MeV)	$r_o$ (fm)	$a_o$ (fm)	$W_v$ (MeV)	$r_v$ (fm)	$a_v$ (fm)	$W_s$ (MeV)	$r_s$ (fm)	$a_s$ (fm)	$V_{s,o}$ (MeV)	$r_{s,o}$ (fm)	$a_{s,o}$ (fm)	Ref.
${}^4\text{He}$	40.0	51.0	1.100	0.350				4.19	2.390	0.10	2.75	1.100	0.350	[16]
${}^4\text{He}$	45.0	49.6	1.100	0.350				5.94	2.320	0.10	2.17	1.100	0.350	[16]
${}^6\text{He}$	41.6	26.0	1.249	0.997	25.0	1.500	0.500	0.30	1.310	0.36	6.00	1.249	0.797	(this work)

For  $p+{}^4\text{He}$  elastic scattering, at 40 and 45 MeV (Fig. 1(d), (e)), the best fit parameters are taken from the existing literature [16] in which the volume imaginary part ( $W_V$ ) is zero and the non-zero surface imaginary part ( $W_S$ ) has large radius ( $r_S \geq 2.3$  fm). For the  ${}^6\text{He} + p$  data at 41.6 MeV (Fig. 1(f)), the search was carried out starting from the OM parameters available for the  ${}^6\text{Li}(p, p)$  scattering [17]. Unlike the  ${}^4\text{He}(p, p)$  scattering, both  $W_S$  and  $W_V$  contribute in  $p({}^6\text{He}, {}^6\text{He})$ , the best fit necessitating larger potential radius ( $r_V$ ) and diffusivity ( $a_0, a_V$ ) compared to those of  ${}^6\text{Li}(p, p)$ .

In semi-microscopic analysis, the real part of the optical potential is replaced by the folded potential, and a search on the phenomenological imaginary potentials is again carried out starting from the above parameters. In  $p+{}^4\text{He}$ , the parameter  $W_S$  had to be decreased from 4.19 to 1.50 at 40 MeV, and from 5.94 to 2.00 at 45 MeV incident energy. The radius  $r_S$  had to be changed from 2.32 fm to 2.40 fm for the latter. In both cases the microscopic real part of the potential did not require any renormalization factors, indicating no measurable breakup channel coupling effect for the tightly bound  ${}^4\text{He}$  nucleus. But, for the 41.6 MeV  ${}^6\text{He} + p$ ,  $N_R = 0.8$  was essential and  $r_V$  had to be increased from 1.5 fm to 1.6 fm.

In the fully microscopic approach, the 40 MeV and 45 MeV data for  $p+{}^4\text{He}$  scattering are well reproduced by putting  $N_R = 1.0$ ,  $N_I = 0.08$  (Fig. 2(a), (b)). For the  ${}^6\text{He} + p$  scattering, the required value of  $N_R$  is 0.9 and that of  $N_I$  is 0.9 for the P1 model ( $R_m({}^6\text{He}) = 2.32$  fm), and 0.7 for the C model ( $R_m({}^6\text{He}) = 2.76$  fm) shown in Fig. 2(c). All the other density prescriptions ( $N_I \sim 0.7$  to 0.9) gave fits which lie in between the fits from the P1 and C models. As shown in the inset of Fig. 2(c), the density distributions differ significantly in the tail region. The tail part is expected to contribute in the forward angle  ${}^6\text{He} + p$  elastic scattering data, which is distinctly different from  ${}^4\text{He}+p$  scattering at nearby energies (Fig. 1(d)–(f)). Although different density prescriptions do give somewhat different cross sections in the forward angle region, none of them fits the  ${}^6\text{He} + p$  experimental data better than others (Fig. 2(c)) and the difference amongst them is also very small. This is possibly due to extremely small density of  ${}^6\text{He}$  at large radius. In view of this reduced importance of the thin halo part in 41.6 MeV

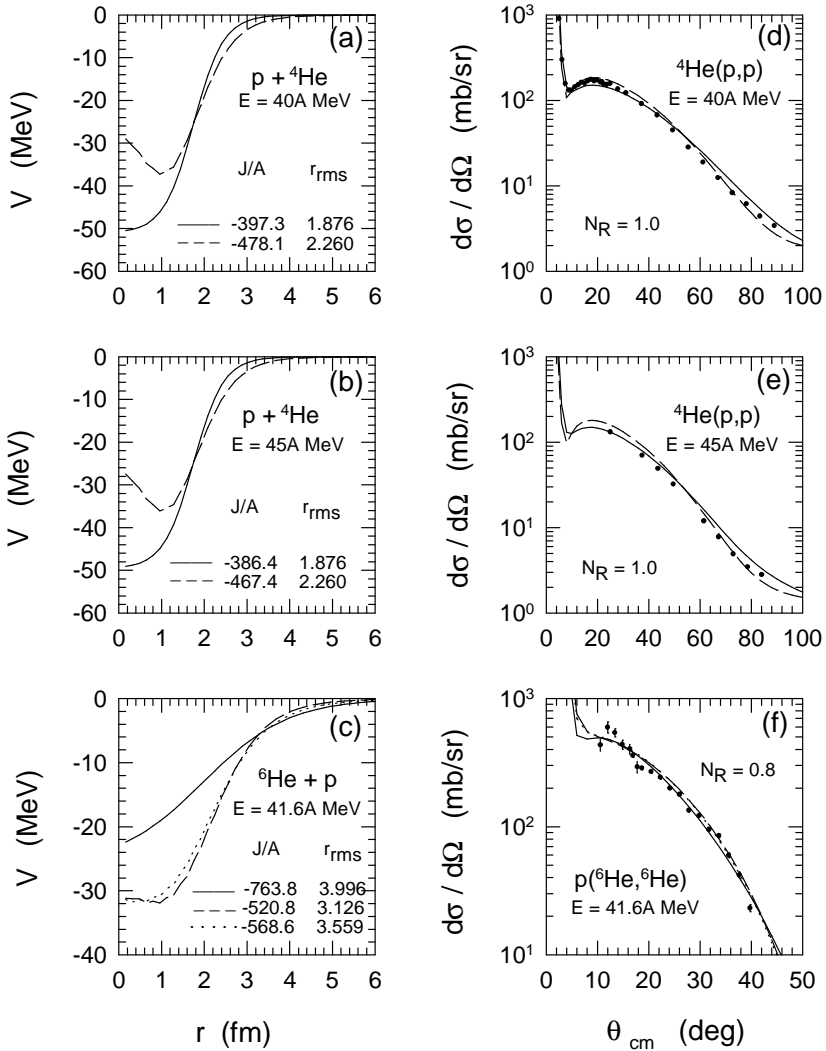


Fig. 1. The real part of the phenomenological (solid) and the renormalized SBM potential (dashed) for the interaction of (a) —  $p+{}^4\text{He}$  at 40A MeV, (b) —  $p+{}^4\text{He}$  at 45A MeV, (c) —  ${}^6\text{He} + p$  at 41.6A MeV. The corresponding elastic scattering angular distributions are shown in (d), (e), (f), where the solid(dashed) line is the result of the phenomenological(semi-microscopic) optical model calculations. In (c) and (f) the dashed(dotted) line correspond to calculation using P1(C) model. The volume integral ( $J/A$ ) of the real part of the potential in  $\text{MeV fm}^3$  and rms radii in fm are shown.

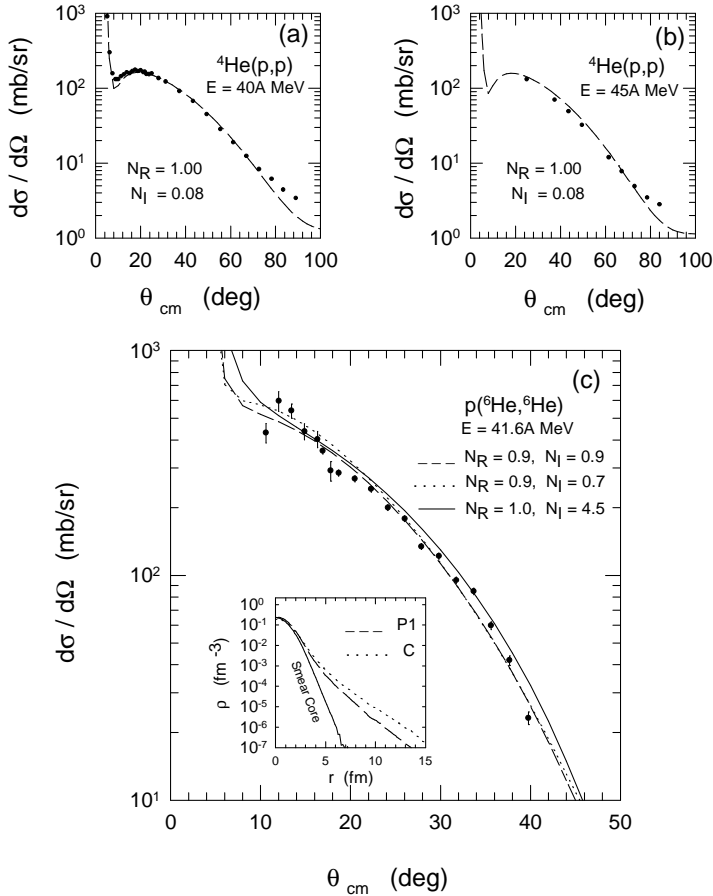


Fig. 2. Same as Fig. 1(d)–(f), but using microscopic real and imaginary potentials. In (c), the calculation using only the smeared-core density of the P1 model is shown by the solid line. The inset in (c) shows the density profiles of the P1 and C models of  ${}^6\text{He}$ . All other density prescriptions lie in between. The smear core density (solid line) corresponding to the P1 model is also shown.

elastic  ${}^6\text{He} + p$  scattering, a microscopic calculation is carried out with the proton scattering from the smeared  ${}^4\text{He}$ -core in  ${}^6\text{He}$ , totally ignoring the halo. Interestingly, the experimental 41.6A MeV  $p({}^6\text{He}, {}^6\text{He})$  data could be reproduced with 41.6A MeV smeared- ${}^4\text{He} + p$  calculations if  $N_I = 4.5$  is used, keeping  $N_R = 1.0$ .

### 3. Conclusions

It is pertinent to note that the 41.6A MeV  ${}^6\text{He} + p$  experimental angular distribution is distinctly different from the  $p + {}^4\text{He}$  at nearby energies, specially at forward angles, where the tail part of the wave functions contribute. However, as all the density prescriptions used in our analysis gave almost same overall fit to the experimental data (Fig. 2(c)), with slight variations of  $N_I$  (0.7 to 0.9), the exact value of the rms radius of  ${}^6\text{He}$  could not be pinpointed. The 41.6A MeV  ${}^6\text{He} + p$  data require renormalizations on the real part of the folded potentials, and possibly indicates significant breakup channel coupling effect on the elastic channel.

An important finding was that if the halo part of  ${}^6\text{He}$  is totally ignored, scattering of protons with the smeared core can also explain the data. This observation indicates that the  ${}^4\text{He}$  core plays a significant role in 41.6A MeV  ${}^6\text{He} + p$  scattering. But total absence of the 2n-halo contribution is possibly not the correct picture as the experimental data could not be fitted unless a large  $N_I$  value is chosen along with  $N_R = 1.0$ . Obviously different  $N_I$  factors associated with different density prescriptions predict different reaction cross-sections. Therefore, experimental data on proton induced  ${}^6\text{He}$ -breakup reactions or, angular distribution data of inelastic proton scattering from  ${}^6\text{He}$  are needed for a better understanding of the structure of the halo nucleus  ${}^6\text{He}$ .

The authors acknowledge M.D. Cortina-Gil for kindly sending the experimental data in a tabular form. The authors also acknowledge Ian Thompson for providing the  ${}^6\text{He}$  densities. Authors R.K acknowledges RIKEN for kind hospitality and D.G acknowledges CSIR, India for financial support.

### REFERENCES

- [1] I. Tanihata, H. Hamagaki, O. Hashimoto, Y. Shida, N. Yoshikawa, K. Sugimoto, O. Yamakawa, T. Kobayashi, N. Takahashi, *Phys. Rev. Lett.* **55**, 2676 (1985).
- [2] P.G. Hansen, B. Jonson, *Europhys. Lett.* **4**, 409 (1987).
- [3] I. Tanihata, *J. Phys. G: Nucl. Part. Phys.* **22**, 157 (1996).
- [4] I. Tanihata, D. Hirata, T. Kobayashi, S. Shimoura, K. Sugimoto, H. Toki, *Phys. Lett.* **B289**, 261 (1992).
- [5] F. Ajzenberg-Selove, *Nucl. Phys.* **A490**, 1 (1988).
- [6] J.S. Al-Khalili, J.A. Tostevin, I.J. Thompson, *Phys. Rev.* **C54**, 1843 (1996).
- [7] I.J. Thompson (private communication).
- [8] Attila Csoto, *Phys. Rev.* **C49**, 3035 (1994).

- [9] J. Jaanecke, T. Annakkage, G.P.A. Berg, B.A. Brown, J.A. Brown, G. Crawley, S. Danczyk, M. Fujiwara, D.J. Mercer, K. Pham, D.A. Roberts, J. Stasko, J.S. Winfield, G.H. Yoo, *Phys. Rev.* **C54**, 1070 (1996).
- [10] M.D. Cortina-Gil, P. Roussel-Chomaz, N. Alamanos, J. Barrette, W. Mittig, F.S. Dietrich, F. Auger, Y. Blumenfeld, J.M. Casandjian, M. Chartier, V. Fekou-Youmbi, B. Fernandez, N. Frascaria, A. Gillibert, H. Laurent, A. Lepine-Szily, N.A. Orr, J.A. Scarpaci, J.L. Sida, T. Suomijarvi, *Phys. Lett.* **B401**, 9 (1997).
- [11] Morton K. Brussel, John H. Williams, *Phys. Rev.* **106**, 286 (1957).
- [12] K. Imai, K. Hatanaka, H. Shimizu, N. Tamura, K. Egawa, K. Nisimura, T. Saito, H. Sato, Y. Wakuta, *Nucl. Phys.* **A325**, 397 (1979).
- [13] D.Bandyopadhyay, C. Samanta, S.K. Samaddar, J.N. De, *Nucl. Phys.* **A511**, 1 (1990).
- [14] M.V. Zhukov, D.V. Fedorov, B.V. Danilin, J.S. Vaagen, J.M. Bang, I.J. Thompson, *Nucl. Phys.* **A552**, 353 (1993).
- [15] C. Samanta, Y. Sakuragi, M. Ito, M. Fujiwara, *J. Phys. G: Nucl. Part. Phys.* **23**, 1697 (1997) (See references therein).
- [16] G.E. Thompson, M.B. Epstein, Tatsuro Sawada, *Nucl. Phys.* **A142**, 571 (1970).
- [17] C.M. Perey, F.G. Perey, *Atomic Data and Nuclear Data Tables* **17**, 1 (1976).